Astronomy & Astrophysics

LETTER TO THE EDITOR

SN 2021foa, a transitional event between a Type IIn (SN 2009ip-like) and a Type Ibn supernova

A. Reguitti[1,2,3] , A. Pastorello[3] , G. Pignata[1,2], M. Fraser[4] , M. D. Stritzinger[5] , S. J. Brennan[4], Y.-Z. Cai[6] ,
N. Elias-Rosa[3,7], D. Fugazza[8], C. P. Gutierrez[9,10] , E. Kankare[10,11], R. Kotak[10], P. Lundqvist[12,13],
P. A. Mazzali[14,15], S. Moran[10], I. Salmaso[3,16], L. Tomasella[3] , G. Valerin[3,16], and H. Kuncarayakti[10,9]

(Affiliations can be found after the references)

ABSTRACT

We present photometric and spectroscopic data of the unusual interacting supernova (SN) 2021foa. It rose to an absolute magnitude peak of $M_r = -18$ mag in 20 days. The initial light curve decline shows some luminosity fluctuations before a long-lasting flattening. A faint source ($M_r \sim -14$ mag) was detected in the weeks preceding the main event, showing a slowly rising luminosity trend. The r-band absolute light curve is very similar to those of SN 2009ip-like events, with a faint and shorter duration brightening ('Event A') followed by a much brighter peak ('Event B'). The early spectra of SN 2021foa show a blue continuum with narrow ($\sim$400 km s^{-1}) H emission lines that, two weeks later, reveal a complex profile, with a narrow P Cygni on top of an intermediate-width ($\sim$2700 km s^{-1}) component. At +12 days, metal lines in emission appear and He I lines become very strong, with He I λ5876 reaching half of the Hα luminosity, much higher than in previous SN 2009ip-like objects. We propose that SN 2021foa is a transitional event between the H-rich SN 2009ip-like SNe and the He-rich Type Ibn SNe.

Key words. supernovae: general – supernovae: individual: SN 2021foa

1. Introduction

Supernovae (SNe) that explode within a dense and massive circumstellar medium (CSM) are called 'interacting' SNe (Fraser 2020). If the CSM is H-rich, they are Type IIn SNe (Schlegel 1990; Filippenko 1997), and their spectra show narrow Balmer emission lines. If the CSM is He-rich, they are classified as Type Ibn SNe (Matheson et al. 2000; Pastorello et al. 2008a; Hosseinzadeh et al. 2017), and strong emissions from He I lines are present.

Among SNe IIn, SN 2009ip (Pastorello et al. 2013; Fraser et al. 2013, 2015; Margutti et al. 2014; Mauerhan & Williams 2014; Graham et al. 2014, 2017) and similar objects[1] are characterised by a wide variability or recurrent outbursts in the years prior to the explosion. SN 2009ip has a double-peak light curve with a first luminous ($M_r \sim -15$ mag) maximum just a few weeks before the brightest one ($M_r \sim -18$ mag). These peaks are often referred to as 'Event A' and 'B', respectively (Pastorello et al. 2013).

The second major class of interacting SNe are Type Ibn. Their light curves usually fade rapidly after peaking, and their spectra are dominated by narrow lines of He I and very weak or no H lines. Transitional Type Ibn/IIn SNe that show both H and He I lines, with the He lines having strengths comparable to the H ones, have also been discovered (Pastorello et al. 2008b, 2015; Smith & Mauerhan 2012; Hosseinzadeh et al. 2017).

In this Letter we present the photometric and spectroscopic follow-up campaign of SN 2021foa, an interacting SN with a photometric evolution almost identical to SN 2009ip-like objects. It has a complex Hα line profile, but also strong He I emission lines.

2. Discovery and host galaxy

SN 2021foa (also known as ASASSN-21dg, ATLAS21htp, and PS21cae) was discovered by the All Sky Automated Survey for SuperNovae (ASAS-SN; Shappee et al. 2014) on 15 March 2021 (MJD = 59288.45) at a Sloan-g apparent magnitude of 15.9, with the last non-detection 10 days earlier, at $g = 17.9$ mag (Stanek & Kochanek 2021). However, ASAS-SN detected it on 9 March at $g = 17.6$ mag and observed a six-day rise to $g = 15.9$ mag[2], when the discovery was reported. Its coordinates are $\alpha = 13^h17^m12.29$, $\delta = -17\degree15'24.19$ (J2000). SN 2021foa was classified by Angus (2021). The host galaxy IC 863 is a barred spiral, with a redshift of $z = 0.008386$ (Pisano et al. 2011). The NASA/IPAC Extragalactic Database[3] reports a kinematic distance, corrected for the Virgo infall, of $d = 34.8 \pm 2.4$ Mpc ($\mu = 32.71 \pm 0.15$ mag), which we adopt as the distance to IC 863. The Milky Way reddening towards IC 863 is $A_V = 0.224$ mag (Schlafly & Finkbeiner 2011). From spectroscopic considerations (see Appendix A) we infer the presence of an additional host galaxy extinction of A_V(host) $\approx 0.40 \pm 0.05$ mag.

3. Photometric evolution

Our multi-band follow-up campaign started soon after the discovery and lasted for 6 months. We collected *Swift* ultraviolet

---

[1] SN 2010mc (Smith et al. 2014), SN 2011fh (Pessi et al. 2022), LSQ13zm (Tartaglia et al. 2016), SN 2015bh (Elias-Rosa et al. 2016; Thöne & de Ugarte Postigo 2017), SN 2016bdu (Pastorello et al. 2018), and AT 2016jbu (Kilpatrick et al. 2018; Brennan et al. 2022a,b).

[2] From the ASAS-SN Supernova Patrol.

[3] https://ned.ipac.caltech.edu/
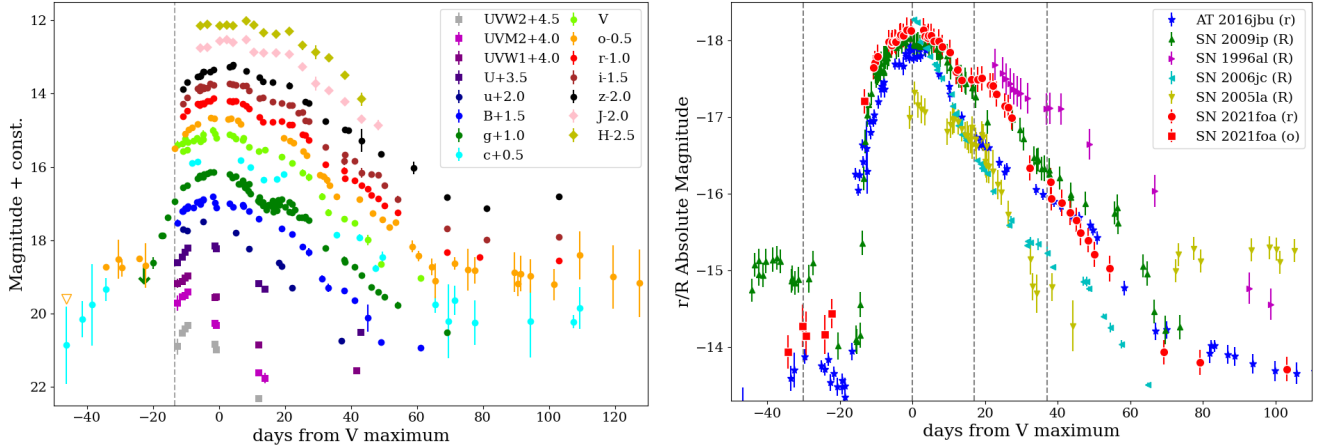
Fig. 1. Light curves of SN 2021foa. *Left*: UV, optical, and NIR light curves of SN 2021foa, covering 6 months of observations. The phases are relative to the *V*-band maximum. The pre-discovery detections are also reported. The discovery epoch is marked with a vertical line. *Right*: comparison of the *r*-band absolute light curves of SN 2021foa, AT 2016jbu, and SN 2009ip (*R*-band). The error bars include the uncertainties on the photometric measurements, the distance, and the reddening in quadrature. The vertical lines mark the significant phases: 'Event A', 'Event B', the 'plateau', and the 'knee'. The ATLAS pre-discovery orange-band detections of SN 2021foa are also shown with square symbols to point out its Event A. The *R*-band absolute light curves of the Type IIn SN 1996al, the Type Ibn SN 2006jc, and the transitional IIn/Ibn SN 2005la are also plotted.

(UV) and ground-based optical and near-infrared (NIR) photometric data with a plethora of telescopes and instruments, which are listed in Table B.1.

The optical and NIR photometric data were reduced using standard procedures with the dedicated SNOoPY pipeline (Cappellaro 2014, see Reguitti et al. 2019 for a description of the procedures). The UV data were reduced with the HEASOFT pipeline[4]. The final UV, optical (Sloan, Johnson, and ATLAS), and NIR magnitudes are listed in Tables B.2–B.6, and the light curves are plotted in the left panel of Fig. 1.

The CHilean Automatic Supernova Search Survey project (Pignata et al. 2009) monitored the field of IC 863 between 2008 and 2015, and the Palomar Transient Factory (Law et al. 2009) scanned it between 2009 and 2014. We inspected their archival images in search of signatures of pre-explosion activity from the progenitor of SN 2021foa but found no evidence of variability. The Pan-STARRS1 (Chambers et al. 2016) survey also observed the sky region of IC 863 in the years 2013–2020, providing only deep (~22 mag) non-detections, which allow us to estimate upper limits to the pre-explosion progenitor's variability. Instead, the Asteroid Terrestrial-impact Last Alert System (ATLAS; Tonry et al. 2018) survey detected the 12-day rise of a faint source (from ATLAS-cyan (*c*) ~20.4 to ~18.8 mag) at the position of SN 2021foa beginning on 10 February 2021, 43 days before the discovery, that then remained nearly constant at ATLAS-orange (*o*) ~19 mag for 3 weeks.

We observed a rise in the first four *Swift* epochs. By fitting a second-order polynomial to the data, we found that the UV maximum was reached about 5 days after discovery, while in the optical the peak was reached between 3 and 6 days later, in the *B* and *z* band, respectively. The *V*-band maximum was reached on MJD = 59301.8 ± 0.1, and we adopted this as a reference epoch. The *V*-band peak absolute magnitude is $M_V = -17.8 \pm 0.2$ mag. The light curves are remarkably similar in the different bands: after maximum, the luminosity of the object starts to decline before settling into a plateau (for ~10 days, between +13 and +22 d) at about 1 mag fainter than the peak (less in redder bands,

e.g., 0.5 mag in *z*). Following the plateau, the light curves display a rapid and linear decline, lasting ~2 months, with a faster decay in the blue filters compared to the red ones. The latest observed magnitudes are slightly fainter than the pre-discovery ATLAS ones. The NIR light curve evolution follows that of the redder optical bands (although the NIR campaign lasted only 2 months). After +80 d, a flattening is observed in the *riz*, cyan, and orange light curves. The ATLAS observations continued up to +130 d, when they were stopped because the object was too close to the Sun.

As shown in the right panel of Fig. 1, we find a remarkable similarity between the *r*-band absolute light curves of SN 2021foa and SN 2009ip during the brightest event (Pastorello et al. 2013; Fraser et al. 2013), as well as with that of the SN 2009ip-like object AT 2016jbu (Kilpatrick et al. 2018; Brennan et al. 2022a). Comparing them with those of the H-rich Type IIn SN 1996al (Benetti et al. 2016), the He-rich SN 2006jc (Pastorello et al. 2007), and the transitional IIn/Ibn SN 2005la (Pastorello et al. 2008b), we see that the decline rate of SN 2021foa is intermediate between the H- and He-rich SNe. The faint ATLAS pre-discovery detections (at $M_o \sim -14$ mag) correspond to the 'Event A', while the brighter post-discovery light curve peak is the 'Event B'. The 'plateau' at +20 d is more pronounced in SN 2021foa, while the 'knee' occurs slightly earlier (+40 d instead of 45 d) and is less noticeable. Finally, both AT 2016jbu and SN 2021foa show a much slower decline in their light curves, roughly from +70 d onwards.

4. Spectral evolution

We also conducted a spectroscopic follow-up of SN 2021foa, during which we collected 19 optical spectra that span the first 3 months of evolution. The log of spectroscopic observations is provided in Table B.7, and the time series is presented in the left panel of Fig. 2. The spectra from the 'Copernico' telescope, the Nordic Optical Telescope (NOT), and the Gran Telescopio Canarias (GTC) were reduced, extracted, and calibrated with slightly different versions of the Foscgui[5] pipeline

---

[4] NASA High Energy Astrophysics Science Archive Research Center – Heasarc 2014.

[5] https://sngroup.oapd.inaf.it/foscgui.html
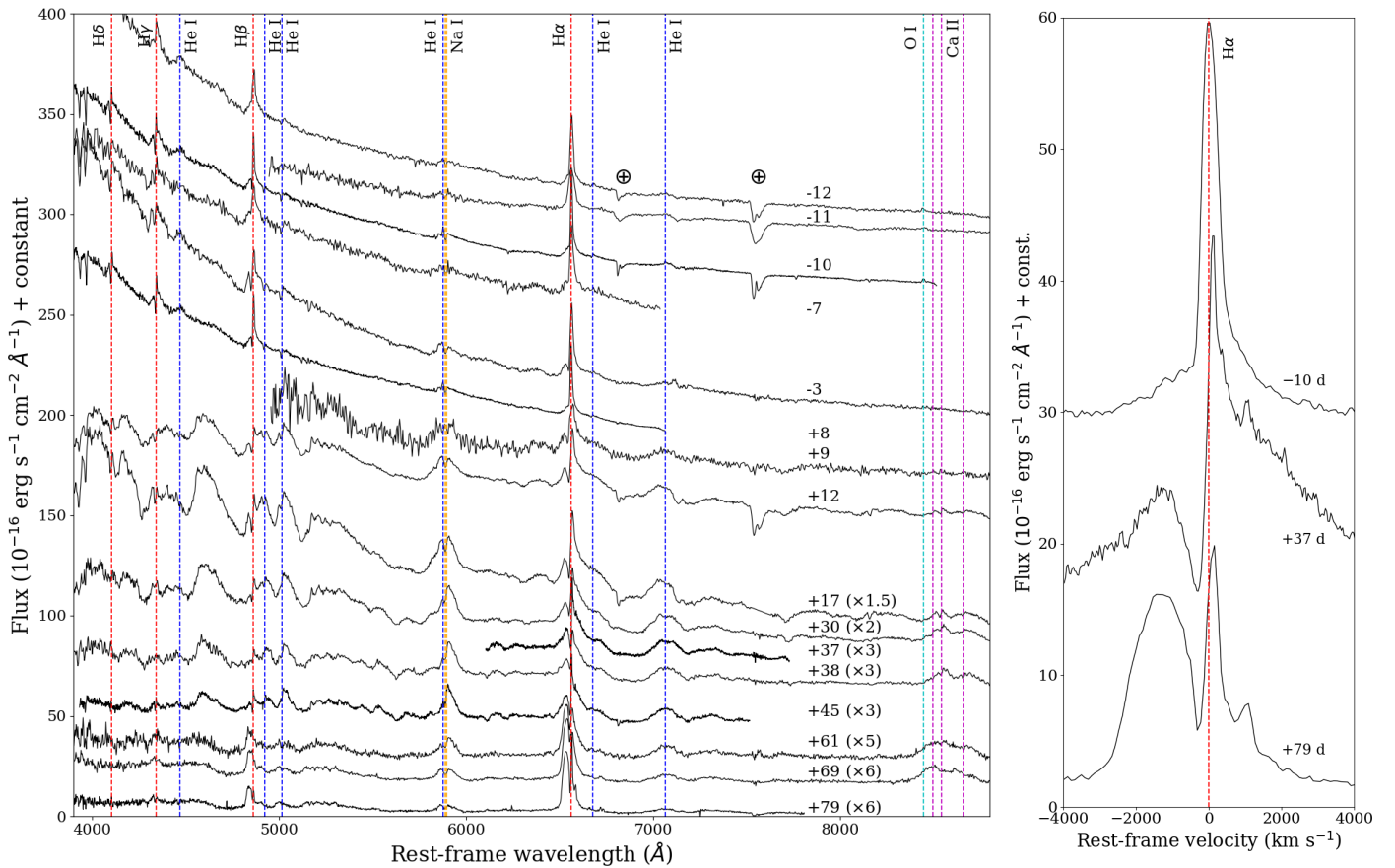
Fig. 2. Spectra of SN 2021foa. *Left*: sequence of spectra of SN 2021foa. The spectra are redshift- and reddening-corrected. The principal identified lines are marked, as are the telluric absorption bands. The phases indicated are relative to the V-band maximum. For a better visualisation, the fluxes of the late spectra are multiplied by the factor reported in parentheses. *Right*: zoomed-in view of the Hα line at three representative epochs, -10 d, $+37$ d, and $+79$ d, to highlight the evolution and the complexity of its profile. In abscissa are the rest-frame velocities.

(Cappellaro 2014), adapted for instruments attached to each telescope. The spectra from the Telescopio Nazionale *Galileo* (TNG) were reduced with the standard procedures under the PyRAF environment. The final spectra were flux-corrected using the nearest, in time, available photometry.

The early spectra show a blue and hot continuum with a black-body temperature, T_{BB}, of 15 000 K and narrow H lines in emission, as typically observed in SNe IIn. He I lines (λ4471, λ5015, and λ5876) are present but weak. Two days later (at -10 d), we took a mid-resolution spectrum. In this spectrum, the Hβ, Hγ, and Hδ lines start to develop a narrow P Cygni absorption on top of the intermediate component. From Hβ, the position of the P Cygni minimum corresponds to an expansion velocity of 500 km s^{-1}. We used the Image Reduction and Analysis Facility (IRAF[6]) task splot to separate the Hα profile into two Gaussian components: a narrow component with a full-width at half maximum (FWHM) velocity[7] of 400 km s^{-1} and an intermediate one of 2700 km s^{-1}.

From the 3 days before the V-maximum spectrum onwards, Hα starts to show a narrow P Cygni absorption profile. At this epoch, T_{BB} has dropped to 12 000 K. Two weeks after the maximum, the spectrum dramatically changes: in the blue part, emission lines from metals appear, mostly with P Cygni profiles (such as the multiplet 42 of Fe II $\lambda\lambda$4924, 5018, and 5169), and He I lines are now very strong, particularly λ5876, with a flux that is close to half that of Hα. A deep absorption feature is visible on top of the He I λ5876 line. The Balmer lines also reveal P Cygni absorptions, up to Hε. The narrow P Cygni absorption of Hα is now evident, and the intermediate-width component has turned into a broad one, with a FWHM velocity (v_{FWHM}) of $\sim$8000 km s^{-1}.

Later, the P Cygni profiles tend to disappear (except Hα), the metal lines broaden, and the He I lines remain strong (at $+12$ d, we measure the following flux ratios: He I λ5876/H$\alpha \simeq 1/2$ and He I λ7065/H$\alpha \simeq 1/4$). At $+30$ d, the lines become more prominent relative to the continuum and broaden, with a mean v_{FWHM} of $\sim$5000 km s^{-1}. The P Cygni absorption in Hα is less evident, and Hβ weakens. The He I lines are still more prominent than most Balmer lines, and a broad double-peak bump from the Ca II NIR triplet emerges, as does a feature around 7300 Å that can be attributed to [Ca II] $\lambda\lambda$7291, 7324, as its profile is comparable to that of the Ca II NIR triplet or, alternatively, He I λ7281. Furthermore, a broad and strong emission centred at 4600 Å is present in the blue part, possibly due to Fe II. The temperature has cooled to $T \sim 7000$ K, based on the peak of the continuum flux.

In the $+37$ d mid-resolution spectrum, we de-blended Hα into broad emission ($v_{FWHM} \sim 6000$ km s^{-1}), narrow emission

___

[6] IRAF is distributed by the National Optical Astronomy Observatory, which is operated by the Association of Universities for Research in Astronomy (AURA) under a cooperative agreement with the National Science Foundation.

[7] Corrected for instrumental resolution, i.e., $FWHM_{corrected} = \sqrt{FWHM_{observed}^2 - FWHM_{instrument}^2}$.
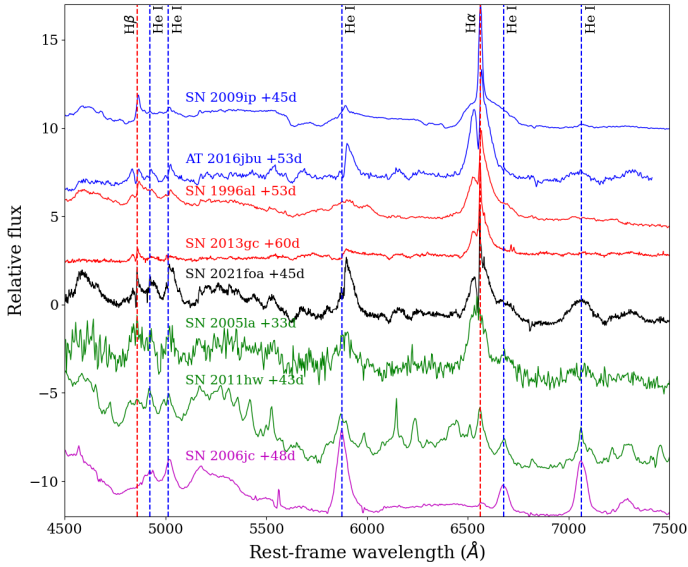
Fig. 3. Spectral comparison at a similar phase (around 1.5 months after the *V*-band maximum) of SN 2021foa, Type IId SNe 2013gc and 1996al, SN 2009ip and the 2009ip-like event AT 2016jbu, the prototypical Type Ibn SN 2006jc, and the transitional Type Ibn/IIn SNe 2005la and 2011hw. Different colours indicate different SN types: SN 2009ip-like in blue, SNe IId in red, transitional IIn/Ibn in green, and Ibn in purple.

($v_{FWHM} \approx 450 \, \mathrm{km \, s^{-1}}$), and a narrow P Cygni absorption, which has a velocity at the minimum position that is consistent with the FWHM of the narrow emission component. A red shoulder of Hα is consistent with the emerging He I λ6678 line. The He I λ7065 line has a trapezoidal shape, with $v_{FWHM} \sim 6000 \, \mathrm{km \, s^{-1}}$. At about 2 months after the maximum, the He I lines weaken, with He I λ5876/Hα $\simeq$ 1/3, and the P Cygni absorption on top of Hα becomes less pronounced.

5. Discussion and conclusion

The complex Balmer emission line profiles in SN 2021foa, especially Hα (Fig. 2, right panel), with the simultaneous presence of multiple emission components and a narrow P Cygni absorption, are a distinctive characteristic of a subclass of SNe IIn sometimes labelled as SNe IId (Benetti 2000; Benetti et al. 2016; Reguitti et al. 2019). SN 2009ip-like events also reveal a similar structured profile, though they do not show strong He I lines. In Fig. 3 we compare the spectral region 4500–7500 Å of SN 2021foa, two SNe IId (SNe 2013gc and 1996al), SN 2009ip (Pastorello et al. 2013), and AT 2016jbu (Brennan et al. 2022a) at about 1.5 months after the *V*-band maximum. We note that the Hα profiles are quite similar, while the He I lines in SN 2021foa are much stronger than those of the comparison objects.

Conversely, the blue part of the spectra of SN 2021foa and the strength of the He I lines resemble those of He-rich Type Ibn SNe (Pastorello et al. 2007; Hosseinzadeh et al. 2017). Two notable objects are SN 2011hw (Smith & Mauerhan 2012; Pastorello et al. 2015), a transitional SN Ibn/IIn that shows an Hα emission in an otherwise He-dominated spectrum, and SN 2005la (Pastorello et al. 2008b), in which Hα is even stronger than the He lines. In both objects, an Ofpe/WN9, in transition from a luminous blue variable (LBV) to an early H-poor but not H-free Wolf-Rayet (WR) star, was suggested as a progenitor. In the lower part of Fig. 3, SN 2021foa is com-

pared with the Type Ibn SN 2006jc (Pastorello et al. 2007) and the transitional IIn/Ibn SNe 2005la and 2011hw. These objects show a progressive strengthening of the Hα emission, though the He I lines remain prominent. SN 2021foa may be part of a bridge connecting H-rich SN 2009ip-like and Type Ibn SN events, indicating the possible existence of a continuum in properties, mass-loss history, and progenitor types between these two types of peculiar transients. The host galaxy metallicity plays an important role in the mass-loss history of massive stars, as a metal-poor environment is expected to inhibit mass loss in massive stars, in contrast with what happens with metal-rich environments. Indeed, the metallicity near the site of SN 2021foa (see Appendix A) is roughly solar.

The outer envelope of the progenitor of SN 2021foa was still H-rich, as at late phases Hα emission remains the predominant spectral feature, but a larger fraction was lost with respect to SN 2009ip. The suggested progenitors of SN 2009ip-like events are H-rich LBV stars (Smith et al. 2010, 2014; Foley et al. 2011b; Mauerhan & Smith 2013, but see Brennan et al. 2022b). Type IId SNe are probably connected to those objects by having similar progenitors, but they probably have a different mass-loss history or are observed with a different orientation. The supposed progenitors of SNe Ibn are H-poor WR stars (Foley et al. 2011a), but Sun et al. (2020) concluded that SNe Ibn can originate from lower-mass stars ($M < 12 \, M_\odot$) in interacting binaries. The detonation of a helium white dwarf scenario was also proposed (Sanders et al. 2013; Hosseinzadeh et al. 2019). As SN 2021foa shares photometric and spectroscopic properties with SN 2009ip and SNe IId, but with strong He I lines that resemble the spectra of IIn/Ibn SNe, the progenitor of SN 2021foa could have been an LBV on the way to becoming a WR star. The star has likely lost a large fraction of its H envelope, although a residual H layer is still retained. The wind velocity derived from Hα ($\sim$450 km s^{-1}) is relatively low for a classical WR. While this is consistent with the wind velocity from an LBV (e.g., Vink 2018), it is also compatible with the wind from a WNH star (Smith 2017) and is similar to that observed for SN 2005la (Pastorello et al. 2008b).

The upcoming 10-year Legacy Survey of Space and Time at the *Vera Rubin* Telescope will discover hundreds of transitional objects. Statistical studies of transients similar to SN 2021foa and their environments will enable us to elucidate their uncertain nature.

References

Angus, C. 2021, TNSCR, 1133
Asplund, M., Grevesse, N., Sauval, A. J., et al. 2009, ARA&A, 47, 481
Benetti, S. 2000, Mem. Soc. Astron. It., 71, 323
Benetti, S., Chugai, N. N., Utrobin, V. P., et al. 2016, MNRAS, 456, 3296
Brennan, S. J., Fraser, M., Johansson, J., et al. 2022a, MNRAS, 513, 5642
Brennan, S. J., Fraser, M., Johansson, J., et al. 2022b, MNRAS, 513, 5666
Cappellaro, E. 2014, http://sngroup.oapd.inaf.it/snoopy.html
Chambers, K. C., Magnier, E. A., Metcalfe, N., et al. 2016, ArXiv e-prints [arXiv:1612.05560]
Dopita, M. A., Kewley, L. J., Sutherland, R. S., et al. 2016, Ap&SS, 361, 61
Elias-Rosa, N., Pastorello, A., Benetti, S., et al. 2016, MNRAS, 463, 3894
Filippenko, A. V. 1997, ARA&A, 35, 309
Foley, R. J., Smith, N., Ganeshalingam, M., et al. 2011a, ApJ, 657, 105
Foley, R. J., Berger, E., Fox, O., et al. 2011b, ApJ, 732, 32
Fraser, M. 2020, RSOS, 700467
Fraser, M., Inserra, C., Jerkstrand, A., et al. 2013, MNRAS, 433, 1312
Fraser, M., Kotak, R., Pastorello, A., et al. 2015, MNRAS, 453, 3886
Graham, M. L., Sand, D. J., Valenti, S., et al. 2014, ApJ, 787, 163
Graham, M. L., Bigley, A., Mauerhan, J. C., et al. 2017, MNRAS, 469, 1559
Hosseinzadeh, G., Arcavi, I., Valenti, S., et al. 2017, ApJ, 836, 158
Hosseinzadeh, G., McCully, C., Zabludoff, A. I., et al. 2019, ApJ, 871, 9
Kilpatrick, C. D., Foley, R. J., Drout, M. R., et al. 2018, MNRAS, 473, 4805
Lagattuta, D. J., Mould, J. R., Staveley-Smith, L., et al. 2013, ApJ, 771, 88
Law, N. M., Kulkarni, S. R., Dekany, R. G., et al. 2009, PASP, 121, 1395
Margutti, R., Milisavljevic, D., Soderberg, A. M., et al. 2014, ApJ, 780, 21
Marino, R. A., Rosales-Ortega, F. F., Sànchez, S. F., et al. 2013, A&A, 559, A114
Matheson, T., Filippenko, A. V., Chornock, R., et al. 2000, AJ, 119, 2303
Mauerhan, J. C., Smith, N., Filippenko, A. V., et al. 2013, MNRAS, 430, 1801
Mauerhan, J. C., Williams, G. G., Smith, N., et al. 2014, MNRAS, 442, 1166
Pastorello, A., Smartt, S. J., Mattila, S., et al. 2007, Nature, 447, 829
Pastorello, A., Mattila, S., Zampieri, L., et al. 2008a, MNRAS, 389, 113
Pastorello, A., Quimby, R. M., Smartt, S. J., et al. 2008b, MNRAS, 389, 131
Pastorello, A., Cappellaro, E., Inserra, C., et al. 2013, ApJ, 767, 1
Pastorello, A., Benetti, S., Brown, P. J., et al. 2015, MNRAS, 449, 1921
Pastorello, A., Wang, X.-F., Ciabattari, F., et al. 2016, MNRAS, 456, 853
Pastorello, A., Kochanek, C. S., Fraser, M., et al. 2018, MNRAS, 474, 197
Pessi, T., Prieto, J. L., Monard, B., et al. 2022, ApJ, 928, 138
Pignata, G., Maza, J., Antezana, R., et al. 2009, AIP Conf. Ser., 1111, 551
Pisano, D. J., Barnes, D. G., Staveley-Smith, L., et al. 2011, ApJS, 197, 28
Poznanski, D., Prochaska, J. X., & Bloom, J. S. 2012, MNRAS, 426, 1465
Reguitti, A., Pastorello, A., Pignata, G., et al. 2019, MNRAS, 482, 2750
Sanders, N. E., Soderberg, A. M., Foley, R. J., et al. 2013, ApJ, 769, 39
Schlafly, E. F., & Finkbeiner, D. P. 2011, ApJ, 737, 103
Schlegel, E. M. 1990, MNRAS, 244, 269
Shappee, B., Prieto, J. L., Stanek, K. Z., et al. 2014, A&AS, 2232, 3603
Smith, N., Miller, A., Li, W., et al. 2010, AJ, 139, 1451
Smith, N., Mauerhan, J. C., Silverman, J. M., et al. 2012, MNRAS, 426, 1905
Smith, N., Mauerhan, J. C., & Prieto, J. L. 2014, MNRAS, 438, 1191
Smith, N. 2017, in Handbook of Supernovae, eds. A. W. Alsabti, & P. Murdin, 403
Spergel, D. N., Bean, R., Doré, O., et al. 2007, ApJS, 170, 377
Stanek, K. Z., & Kochanek, C. S. 2021, TNSTR, 767
Sun, N.-C., Maund, J. R., Hirai, R., et al. 2020, MNRAS, 491, 6000
Tartaglia, L., Pastorello, A., Sullivan, M., et al. 2016, MNRAS, 459, 1039
Thöne, C. C., de Ugarte Postigo, A., Leloudas, G., et al. 2017, A&A, 599, A129
Tonry, J. L., Denneau, L., Heinze, A. N., et al. 2018, PASP, 130, 4505
Turatto, M., Benetti, S., & Cappellaro, E. 2003, in From Twilight to Highlight: The Physics of Supernovae: Proceedings of the ESO/MPA/MPE Workshop Held at Garching, eds. W. Hillebrandt, & B. Leibundgut (Berlin: Springer-Verlag), 200
Vink, J. S. 2018, A&A, 619, A54

[1] Departamento de Ciencias Físicas – Universidad Andres Bello, Avda. República 252, 8320000 Santiago, Chile
e-mail: andreareguitti@gmail.com

[2] Millennium Institute of Astrophysics, Nuncio Monsenor Sótero Sanz 100, Providencia 8320000, Santiago, Chile

[3] INAF – Osservatorio Astronomico di Padova, Vicolo dell'Osservatorio 5, 35122 Padova, Italy

[4] School of Physics, O'Brien Centre for Science North, University College Dublin, Belfield, Dublin 4, Ireland

[5] Department of Physics and Astronomy, Aarhus University, Ny Munkegade 120, 8000 Aarhus C, Denmark

[6] Physics Department and Tsinghua Center for Astrophysics (THCA), Tsinghua University, Beijing 100084, PR China

[7] Institute of Space Sciences (ICE, CSIC), Campus UAB, Carrer de Can Magrans s/n, 08193 Barcelona, Spain

[8] INAF – Osservatorio Astronomico di Brera, Via E. Bianchi 46, 23807 Merate, Italy

[9] Finnish Centre for Astronomy with ESO (FINCA), University of Turku, Vesilinnantie 5, 20014 Turku, Finland

[10] Department of Physics and Astronomy, University of Turku, 20014 Turku, Finland

[11] Turku Collegium for Science, Medicine and Technology, University of Turku, 20014 Turku, Finland

[12] Department of Astronomy, AlbaNova University Center, Stockholm University, 10691 Stockholm, Sweden

[13] The Oskar Klein Centre, AlbaNova, 10691 Stockholm, Sweden

[14] Astrophysics Research Institute, Liverpool John Moores University, ic2, 146 Brownlow Hill, Liverpool L3 5RF, UK

[15] Max-Planck Institut fur Astrophysik, Karl-Schwarzschild-Str. 1, 85741 Garching, Germany

[16] Dipartimento di Fisica e Astronomia 'G. Galilei' – Universitá di Padova, Vicolo dell'Osservatorio 3, 35122 Padova, Italy

Appendix A: Host galaxy metallicity and reddening

From our long-slit spectroscopy of SN 2021foa at a late phase, we extracted the spectrum of an H II region adjacent to the SN. The spectrum shows typical narrow emission lines from ionised gas, including Hα, [N II], and [S II]. Assuming that the adjacent H II region is representative of the SN explosion site, we measured the emission line flux of Hα and [N II] λ6584 in its spectrum to derive the oxygen abundance as a metallicity proxy, via the N2 index according to the Marino et al. (2013) calibration, and also the [S II] λ6717,6731 doublet for the same purpose using the Dopita et al. (2016) scale. The measured metallicity in 12+log(O/H) is 8.59 dex (N2) and 8.66 dex. Within the typical metallicity calibration error of 0.1-0.2 dex, these values agree with each other. The derived metallicity is thus consistent with being nearly solar (12+log(O/H)$_\odot$ = 8.69 dex; Asplund & Grevesse 2009).

The estimate of the line of sight reddening is a crucial step for the characterisation of a stellar transient. One of the most popular ways to estimate this value is through the detection of narrow interstellar lines. Turatto et al. (2003) proposed inferring the colour excess using a linear relation with the equivalent width (EW) of the Na I $\lambda\lambda$5890,5896 doublet. Poznanski et al. (2012) revised the relation using the individual line components in higher resolution spectra.

In our early spectra of SN 2021foa, a narrow absorption of the Na I doublet is visible on top of the He I λ5876 line at the host galaxy redshift, with EW=0.8±0.1 Å. The Poznanski et al. (2012) relation between sodium absorption and dust extinction saturates at EWs beyond 0.8 Å, and hence we estimated the internal extinction using the Turatto et al. (2003) formula, which provides an additional reddening of $A_V(host) \approx 0.40 \pm 0.05$ mag.

In Fig. A.1 we show the evolution of the profile of the narrow (interstellar) Na I D feature in the velocity space. While its EW remains roughly constant (within the measurement errors) until +45 d, it seems to significantly increase in the late-time spectra. However, the change in the relative intensities of the broader features of He I λ5876 and Na I D (attributed to the SN ejected material) hinders a reliable estimate of the EW of the interstellar Na I D component, and probably explains its apparent evolution without needing to invoke changes in the ionisation state of the interstellar medium. Indeed, in the last spectrum the minimum of the P Cygni absorption component of Na I D is blueshifted by about 400 km s^{-1}, which is about the same amount as in Hα. This indicates that both the narrow interstellar absorption and the P Cygni line of the transient contribute to the observed Na I D profile. As a consequence, in this paper we assume that the EW
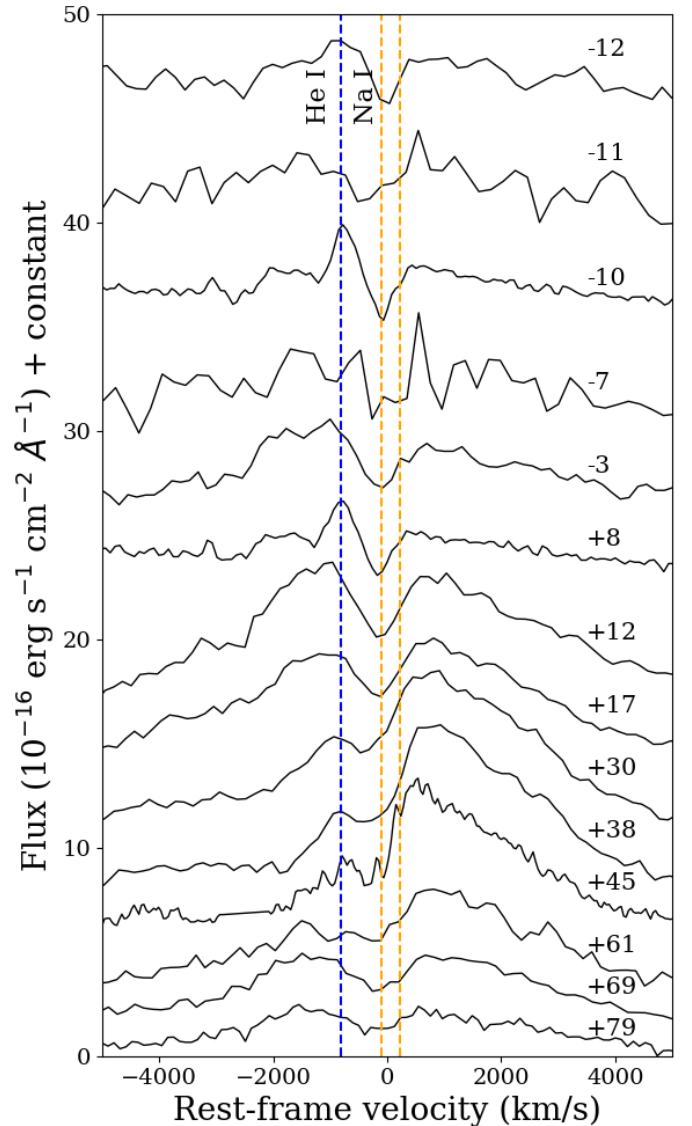
Fig. A.1. Evolution of the profile of the Na I absorption with time, in velocity space.

of the Na I D absorption measured only in the early spectra is entirely produced by interstellar gas and can be used as a proxy to estimate the reddening contribution of the host galaxy.

Appendix B: Tables

Table B.1. Observational facilities and instrumentation used in the photometric follow-up of SN 2021foa.

Telescope	Location	Instrument	Filters
Swift (0.3m)	Space	UVOT	*UV* filters+*UBV*
ASAS-SN (0.14m)	Texas	"Leavitt"	*g*
PROMPT (0.4m+0.6m)	CTIO	Apogee	*BVgriz*
ATLAS (0.5m)	Hawaii	ACAM1	*c, o*
REM (0.6m)	La Silla	ROS2	*griz*
Schmidt (0.67m)	Asiago	Moravian	*uBVgri*
Copernico (1.82m)	Asiago	AFOSC	*iz*
LT (2.0m)	La Palma	IO:O	*uBVgriz*
NOT (2.56m)	La Palma	ALFOSC	*uBVgriz*
REM (0.5m)	La Silla	REMIR	*JH*

Table B.2. *Swift* UV magnitudes of SN 2021foa in the Vega system. All measurements are from the Ultraviolet/Optical Telescope (UVOT) instrument.

Date	MJD	$UVW2$	$UVM2$	$UVW1$
2021-03-16	59289.21	16.40±0.22	15.72±0.21	15.18±0.12
2021-03-17	59290.73	16.03±0.04	15.54±0.03	15.12±0.03
2021-03-18	59291.64	15.91±0.04	15.50±0.03	15.03±0.03
2021-03-19	59292.44	15.82±0.03	15.41±0.03	14.98±0.03
2021-03-27	59300.61	16.33±0.05	16.27±0.05	15.57±0.05
2021-03-28	59301.15	16.49±0.06	16.32±0.06	15.55±0.05
2021-04-09	59313.89	17.82±0.09	17.61±0.08	16.86±0.07
2021-04-11	59315.74	-	17.76±0.14	-
2021-05-09	59343.68	-	-	17.55±0.04

Table B.3. Johnson *UBV* VEGA magnitudes of SN 2021foa.

Date	MJD	*U*	*B*	*V*	Instrument
2021-03-16	59289.21	15.12±0.08	16.02±0.09	15.40±0.11	UVOT
2021-03-17	59290.73	14.97±0.06	15.71±0.08	15.37±0.05	UVOT
2021-03-17	59290.99	-	15.71±0.02	15.56±0.03	Moravian
2021-03-18	59291.64	14.83±0.06	15.64±0.05	15.23±0.05	UVOT
2021-03-19	59292.12	-	15.63±0.01	15.53±0.01	IO:O
2021-03-19	59292.44	14.70±0.05	15.58±0.03	15.32±0.04	UVOT
2021-03-21	59294.13	-	15.61±0.08	15.29±0.04	Apogee
2021-03-22	59295.13	-	15.46±0.04	15.21±0.08	Apogee
2021-03-22	59295.97	-	15.44±0.05	15.26±0.03	Moravian
2021-03-23	59296.12	-	15.52±0.05	15.30±0.05	Apogee
2021-03-24	59297.06	-	15.38±0.01	15.25±0.01	IO:O
2021-03-24	59297.12	-	15.39±0.06	15.11±0.11	Apogee
2021-03-27	59300.11	-	15.30±0.07	14.99±0.08	Apogee
2021-03-27	59300.61	14.65±0.04	15.48±0.04	15.10±0.05	UVOT
2021-03-28	59301.15	14.74±0.04	15.60±0.04	15.21±0.06	UVOT
2021-04-01	59305.09	-	15.50±0.04	15.11±0.05	Apogee
2021-04-02	59306.10	-	15.58±0.04	15.15±0.06	Apogee
2021-04-02	59306.95	-	-	15.22±0.02	Moravian
2021-04-04	59308.98	-	15.53±0.02	15.27±0.01	Moravian
2021-04-05	59309.17	-	15.56±0.06	15.21±0.06	Apogee
2021-04-07	59311.02	-	15.70±0.02	15.46±0.02	Moravian
2021-04-09	59313.89	15.68±0.09	15.91±0.04	15.57±0.06	UVOT
2021-04-11	59315.74	15.83±0.09	-	15.53±0.06	UVOT
2021-04-16	59320.95	-	16.19±0.02	15.72±0.03	Moravian
2021-04-19	59323.98	-	16.33±0.02	15.89±0.04	Moravian
2021-04-23	59327.13	-	16.68±0.08	16.16±0.08	Apogee
2021-04-25	59329.04	-	16.83±0.11	16.28±0.10	Apogee
2021-04-29	59333.02	-	17.55±0.09	16.80±0.08	Apogee
2021-05-01	59335.01	-	17.79±0.11	17.24±0.09	Apogee
2021-05-05	59339.89	-	17.88±0.07	17.42±0.08	Moravian
2021-05-08	59342.86	-	18.14±0.05	17.52±0.05	Moravian
2021-05-10	59344.75	17.00±0.03	-	-	UVOT
2021-05-13	59347.03	-	18.62±0.37	17.99±0.14	Apogee
2021-05-16	59350.90	-	19.27±0.04	18.65±0.02	IO:O
2021-05-29	59363.01	-	19.43±0.03	19.02±0.03	ALFOSC

Table B.4. Sloan *ugriz* AB magnitudes of SN 2021foa.

Date	MJD	*u*	*g*	*r*	*i*	*z*	Instrument
2021-03-05	59278.41	-	>17.9	-	-	-	Leavitt
2021-03-09	59282.01	-	17.62±0.16	-	-	-	Leavitt
2021-03-11	59284.87	-	16.87±0.07	-	-	-	Leavitt
2021-03-11	59284.37	-	16.87±0.07	-	-	-	Leavitt
2021-03-13	59286.31	-	16.38±0.05	-	-	-	Leavitt
2021-03-15	59288.45	-	15.93±0.05	-	-	-	Leavitt
2021-03-17	59290.99	15.70±0.02	15.55±0.02	15.61±0.03	15.77±0.03	-	Moravian
2021-03-18	59291.05	-	-	-	-	15.87±0.04	AFOSC
2021-03-19	59292.12	15.74±0.01	15.51±0.01	15.47±0.01	15.61±0.01	15.70±0.01	IO:O
2021-03-22	59295.31	-	15.32±0.02	15.28±0.03	15.36±0.03	15.53±0.05	Apogee
2021-03-22	59295.96	-	15.24±0.04	15.32±0.05	15.41±0.04	-	Moravian
2021-03-23	59296.22	-	15.27±0.02	15.28±0.02	15.40±0.02	15.52±0.03	Apogee
2021-03-23	59296.23	-	15.24±0.02	15.28±0.01	15.31±0.06	15.52±0.10	ROS2
2021-03-24	59297.06	15.49±0.01	15.27±0.01	15.27±0.01	15.32±0.01	15.39±0.01	IO:O
2021-03-24	59297.18	-	15.19±0.02	15.28±0.02	15.35±0.03	15.41±0.03	Apogee
2021-03-25	59298.24	-	15.18±0.03	15.20±0.04	15.33±0.05	-	ROS2
2021-03-26	59299.23	-	15.14±0.03	15.19±0.02	15.22±0.03	15.40±0.03	ROS2
2021-03-27	59300.14	-	15.13±0.02	15.12±0.02	15.25±0.03	15.34±0.04	Apogee
2021-04-01	59305.16	-	15.20±0.01	15.21±0.02	15.23±0.02	15.28±0.03	Apogee
2021-04-02	59306.01	-	15.28±0.02	15.22±0.01	15.24±0.03	15.25±0.04	ROS2
2021-04-02	59306.08	-	15.28±0.02	15.19±0.01	15.24±0.02	15.20±0.02	Apogee
2021-04-02	59306.94	15.80±0.02	15.26±0.02	15.20±0.03	15.26±0.03	-	Moravian
2021-04-03	59307.86	-	15.46±0.03	-	-	-	Leavitt
2021-04-04	59308.20	-	15.46±0.05	-	-	-	Leavitt
2021-04-04	59308.98	-	15.37±0.02	15.27±0.01	15.29±0.02	-	Moravian
2021-04-05	59309.78	-	15.55±0.03	-	-	-	Leavitt
2021-04-06	59310.06	-	15.48±0.03	15.34±0.03	15.28±0.02	15.39±0.05	ROS2
2021-04-06	59310.08	-	15.58±0.03	-	-	-	Leavitt
2021-04-06	59310.78	-	15.65±0.03	-	-	-	Leavitt
2021-04-07	59311.02	16.24±0.03	15.47±0.01	15.41±0.02	15.42±0.03	-	Moravian
2021-04-07	59311.31	-	15.73±0.04	-	-	-	Leavitt
2021-04-09	59313.76	-	15.92±0.04	-	-	-	Leavitt
2021-04-10	59314.09	-	15.96±0.04	-	-	-	Leavitt
2021-04-10	59314.17	-	15.82±0.02	15.64±0.02	15.63±0.02	15.55±0.03	Apogee
2021-04-10	59314.92	-	16.00±0.04	-	-	-	Leavitt
2021-04-11	59315.22	-	16.06±0.04	-	-	-	Leavitt
2021-04-11	59315.27	-	15.96±0.03	15.77±0.03	15.61±0.04	15.67±0.07	ROS2

Table B.4. (Continued) Sloan *ugriz* AB magnitudes of SN 2021foa.

Date	MJD	*u*	*g*	*r*	*i*	*z*	Instrument
2021-04-12	59316.13	-	16.18±0.04	-	-	-	Leavitt
2021-04-12	59316.79	-	16.03±0.05	-	-	-	Leavitt
2021-04-13	59317.12	-	16.03±0.04	-	-	-	Leavitt
2021-04-13	59317.81	-	16.05±0.04	-	-	-	Leavitt
2021-04-14	59318.11	-	16.09±0.05	-	-	-	Leavitt
2021-04-14	59318.41	-	16.22±0.04	-	-	-	Leavitt
2021-04-14	59318.06	-	15.92±0.02	15.77±0.02	15.71±0.02	15.69±0.03	Apogee
2021-04-14	59318.90	-	16.03±0.04	-	-	-	Leavitt
2021-04-15	59319.14	-	15.95±0.03	-	-	-	ROS2
2021-04-15	59319.33	-	16.18±0.05	-	-	-	Leavitt
2021-04-15	59319.87	-	15.90±0.04	-	-	-	Leavitt
2021-04-16	59320.10	16.62±0.02	-	-	-	-	IO:O
2021-04-16	59320.12	-	16.04±0.05	-	-	-	Leavitt
2021-04-16	59320.95	16.71±0.06	15.88±0.02	15.75±0.02	15.76±0.02	-	Moravian
2021-04-17	59321.98	-	16.10±0.05	-	-	-	Leavitt
2021-04-19	59323.11	-	16.23±0.05	-	-	-	Leavitt
2021-04-19	59323.14	-	15.96±0.05	15.84±0.03	15.81±0.05	15.78±0.09	ROS2
2021-04-19	59323.98	17.30±0.08	16.01±0.02	15.84±0.02	15.82±0.03	-	Moravian
2021-04-19	59323.99	-	16.24±0.05	-	-	-	Leavitt
2021-04-20	59324.91	-	16.17±0.04	-	-	-	Leavitt
2021-04-21	59325.96	-	-	-	16.02±0.07	-	AFOSC
2021-04-22	59326.06	-	16.37±0.06	-	-	-	Leavitt
2021-04-22	59326.93	-	16.39±0.07	-	-	-	Leavitt
2021-04-23	59327.14	-	-	16.11±0.03	16.00±0.04	-	ROS2
2021-04-23	59327.93	-	16.36±0.06	-	-	-	Leavitt
2021-04-24	59328.10	-	16.39±0.03	16.13±0.03	16.23±0.04	16.22±0.05	Apogee
2021-04-25	59329.06	-	16.45±0.03	16.26±0.03	16.25±0.05	16.26±0.06	Apogee
2021-04-30	59334.12	-	17.22±0.03	16.92±0.04	16.95±0.05	16.74±0.06	Apogee
2021-05-04	59338.96	18.75±0.02	-	-	-	-	ALFOSC
2021-05-05	59339.89	-	17.53±0.08	17.10±0.10	17.34±0.10	-	Moravian
2021-05-06	59340.11	-	17.59±0.04	17.32±0.03	17.16±0.04	16.99±0.09	ROS2
2021-05-07	59341.01	-	-	-	-	17.01±0.03	ALFOSC
2021-05-08	59342.86	-	17.73±0.04	17.37±0.07	17.34±0.06	-	Moravian
2021-05-11	59345.11	-	17.96±0.08	17.50±0.05	17.66±0.14	17.28±0.32	ROS2
2021-05-12	59346.91	-	-	17.60±0.01	-	-	ALFOSC
2021-05-14	59348.01	-	18.28±0.05	17.76±0.06	17.70±0.07	-	Apogee
2021-05-16	59350.15	-	18.42±0.04	17.86±0.02	17.71±0.04	-	ROS2
2021-05-16	59350.91	-	-	-	-	17.64±0.03	IO:O
2021-05-17	59351.94	-	18.55±0.06	18.05±0.05	18.01±0.04	-	Moravian
2021-05-22	59356.08	-	18.77±0.10	18.23±0.06	18.37±0.09	-	ROS2
2021-05-26	59360.95	-	-	-	-	18.02±0.17	Apogee
2021-06-05	59370.98	-	19.50±0.01	19.32±0.01	19.18±0.01	18.83±0.01	ALFOSC
2021-06-15	59380.93	-	-	19.46±0.04	-	-	OSIRIS
2021-06-17	59382.91	-	-	-	19.48±0.04	19.13±0.04	ALFOSC
2021-07-09	59404.93	-	-	19.55±0.02	19.41±0.04	18.81±0.06	ALFOSC

Table B.5. ATLAS *c* and *o* AB magnitudes of SN 2021foa. The forced photometry is available at `https://fallingstar-data.com/forcedphot`.

Date	MJD	*c*
2021-02-10	59255.51	20.36±1.06
2021-02-15	59260.52	19.65±0.50
2021-02-18	59263.43	19.26±1.11
2021-02-22	59267.52	18.84±0.31
2021-03-20	59293.61	15.40±0.02
2021-03-22	59295.45	15.36±0.02
2021-04-04	59308.46	15.32±0.03
2021-04-07	59311.39	15.51±0.04
2021-04-11	59315.41	15.84±0.05
2021-04-15	59319.39	15.83±0.02
2021-04-17	59321.39	15.70±0.03
2021-05-03	59337.44	17.35±0.06
2021-05-10	59344.37	17.42±0.08
2021-05-15	59349.37	18.26±0.09
2021-05-17	59351.35	17.96±0.16
2021-06-02	59367.35	19.26±0.23
2021-06-06	59371.35	19.71±1.00
2021-06-08	59373.32	19.13±0.40
2021-06-14	59379.34	19.74±0.61
2021-07-01	59396.31	19.70±0.99
2021-07-14	59409.26	19.72±0.18
2021-07-16	59411.25	19.35±0.57

Table B.5. (Continued) ATLAS *c* and *o* AB magnitudes of SN 2021foa.

Date	MJD	*o*
2021-02-10	59255.50	>20.1
2021-02-22	59267.54	19.23±0.05
2021-02-26	59271.46	19.02±0.53
2021-02-27	59272.51	19.25±0.24
2021-03-04	59277.59	19.00±0.08
2021-03-06	59279.53	19.18±0.61
2021-03-15	59288.46	15.99±0.05
2021-03-18	59291.55	15.60±0.02
2021-03-19	59292.54	15.48±0.03
2021-03-20	59293.60	15.43±0.02
2021-03-22	59295.46	15.33±0.03
2021-03-26	59299.45	15.15±0.01
2021-03-27	59300.38	15.17±0.03
2021-03-31	59304.61	15.19±0.04
2021-04-01	59305.55	15.18±0.04
2021-04-03	59307.51	15.24±0.08
2021-04-04	59308.45	15.33±0.02
2021-04-17	59321.39	15.71±0.03
2021-04-19	59323.39	15.79±0.01
2021-04-20	59324.44	15.85±0.02
2021-04-23	59327.44	16.06±0.02
2021-04-24	59328.37	16.18±0.04
2021-04-28	59332.46	16.72±0.05
2021-04-29	59333.50	16.76±0.06
2021-04-30	59334.44	16.85±0.11
2021-05-01	59335.47	17.00±0.08
2021-05-03	59337.43	17.30±0.07
2021-05-10	59344.39	17.38±0.07
2021-05-14	59348.37	17.76±0.06
2021-05-17	59351.36	17.93±0.07
2021-05-19	59353.38	18.14±0.03
2021-05-21	59355.37	18.00±0.07
2021-05-26	59360.41	18.67±0.16
2021-05-28	59362.39	18.93±0.14
2021-06-01	59366.38	19.23±0.23
2021-06-02	59367.34	19.61±0.48
Date	MJD	*o*
2021-06-08	59373.33	19.13±0.18
2021-06-12	59377.32	19.30±0.57
2021-06-14	59379.32	19.32±0.37
2021-06-26	59391.32	19.37±0.54
2021-06-27	59392.33	19.69±0.34
2021-06-28	59393.30	19.41±0.48
2021-07-01	59396.32	19.47±0.46
2021-07-08	59403.32	19.71±0.43
2021-07-16	59411.26	18.91±0.66
2021-07-26	59421.28	19.50±0.87
2021-08-03	59429.27	19.67±0.92

Table B.6. NIR VEGA magnitudes of SN 2021foa. All measurements are from the Rapid Eye Mount-IR instrument.

Date	MJD	J	H
2021-03-23	59296.24	14.75±0.05	14.65±0.07
2021-03-25	59298.24	14.74±0.05	14.61±0.05
2021-03-29	59302.19	14.56±0.10	14.65±0.05
2021-03-31	59304.18	14.53±0.04	14.62±0.05
2021-04-02	59306.01	14.60±0.06	14.65±0.08
2021-04-06	59310.06	14.52±0.06	14.52±0.08
2021-04-08	59312.36	14.87±0.06	14.63±0.11
2021-04-11	59315.28	14.89±0.07	14.84±0.05
2021-04-15	59319.15	14.89±0.04	14.87±0.04
2021-04-19	59323.15	14.93±0.07	14.80±0.05
2021-04-23	59327.15	15.27±0.14	15.18±0.13
2021-04-27	59331.15	15.73±0.19	15.37±0.19
2021-05-01	59335.08	15.91±0.09	15.52±0.11
2021-05-06	59340.11	16.23±0.07	15.99±0.10
2021-05-11	59345.11	16.69±0.12	16.65±0.18
2021-05-16	59350.15	16.86±0.15	-

Table B.7. Log of the spectroscopic observations of SN 2021foa. The phases are relative to the V-band maximum epoch (MJD 59301.8). The spectra will be uploaded to the Weizmann Interactive Supernova Data Repository database at https://www.wiserep.org/.

Date	MJD	Phase (d)	Coverage (Å)	Resolution (Å)	Exposure (s)	Telescope + Instrument + Grism
2021-03-17	59290.0	−12	3800-9000	14	-	NOT+ALFOSC+gr4
2021-03-18	59291.0	−11	5000-9000	40	1200	Copernico+AFOSC+VPH6
2021-03-19	59292.1	−10	3700-8550	6.0	1800	NOT+ALFOSC+gr7/gr8
2021-03-22	59295.0	−7	3900-7100	14	1200	Copernico+AFOSC+VPH7
2021-03-26	59299.1	−3	3600-9650	14	900	NOT+ALFOSC+gr4
2021-04-06	59310.1	+8	3700-7100	6.5	1500	NOT+ALFOSC+gr7
2021-04-06	59310.9	+9	5000-9000	22	900	Copernico+AFOSC+VPH6
2021-04-09	59314.0	+12	3700-9000	18	900	NOT+ALFOSC+gr4
2021-04-14	59319.0	+17	3700-9000	14	1200	NOT+ALFOSC+gr4
2021-04-27	59331.9	+30	3650-9100	13	1500	NOT+ALFOSC+gr4
2021-05-05	59339.0	+37	6150-7750	2.9	1200	TNG+LRS+VHRR
2021-05-06	59340.0	+38	3600-10300	10	600	TNG+LRS+LRB/LRR
2021-05-12	59346.9	+45	4000-7550	3.4	1080	GTC+OSIRIS+R2000B/R2500R
2021-05-28	59362.9	+61	3800-9650	14	2400	NOT+ALFOSC+gr4
2021-06-05	59370.9	+69	3800-9650	14	3600	NOT+ALFOSC+gr4
2021-06-15	59380.9	+79	3700-7850	6.9	1800	GTC+OSIRIS+R1000B